Energy & Environmental Science

RSC Publishing

COMMUNICATION

Biodegradable transparent substrates for flexible organic-light-emitting diodes†

Cite this: *Energy Environ. Sci.*, 2013, **6**, 2105

Received 11th February 2013
Accepted 28th March 2013

DOI: 10.1039/c3ee40492g

www.rsc.org/ees

Hongli Zhu,[a] Zhengguo Xiao,[b] Detao Liu,[c] Yuanyuan Li,[a] Nicholas J. Weadock,[a] Zhiqiang Fang,[a] Jinsong Huang[b] and Liangbing Hu*[a]

Electronics on flexible and transparent substrates have received much interest due to their new functionalities and high-speed roll-to-roll manufacturing processes. The properties of substrates are crucial, including flexibility, surface roughness, optical transmittance, mechanical strength, maximum processing temperature, *etc.* Although plastic substrates have been used widely in flexible macroelectronics, there is still a need for next-generation sustainable, high-performance substrates which are thermally stable with tunable optical properties and a higher handling temperature. In this communication, we focus on cellulose-based transparent, biodegradable substrates incorporating either nanopaper or a regenerated cellulose film (RCF). We found that both their optical and mechanical properties are dramatically different due to the difference of their building blocks. Highly flexible organic-light-emitting diodes (OLEDs) are also demonstrated on the biodegradable substrates, paving the way for next-generation green and flexible electronics.

Broader context

The development and implementation of green electronics incorporating natural materials is key to providing a more sustainable future. One of the main components of electronic devices is the substrate, which provides support for building devices. Properties of the substrate ultimately determine if the device will be flexible or rigid, transparent or opaque, and what manufacturing method will be optimal for large scale device fabrication. The transition from rigid glass to flexible plastic substrates allowed for the creation of flexible, transparent devices that can be produced at high throughput using established roll-to-roll printing methods. Plastic substrates, however, are not produced from sustainable sources and have limited recyclability. We envision that a new transition will replace plastic with materials made from natural sources. These substrates will retain all of the desirable properties of plastic substrates, with the added advantages of being recyclable, renewable, and inexpensive. Investigating the fundamental properties of cellulose as a building block and demonstrating operable devices fabricated on these substrates are important steps in catalyzing the shift from plastic to natural materials.

Introduction

Roll-to-roll processed flexible electronics have potential applications in military and consumer electronics as they are low-cost and possess unprecedented properties.[1–4] Various devices have been successfully demonstrated on plastic substrates including transistor backplanes, thin film transistors, organic light emitting diodes and others. Plastic substrates such as polyethylene terephthalate (PET), polyethylene naphthalate (PEN), polycarbonate (PC), and polyimide (PI) have been used.[5–11] The substrate is crucial for flexible electronics since it (1) provides mechanical support, (2) enables roll-to-roll device fabrication, and (3) is the first layer in the device to allow for manipulation of photons and electrons for achieving tailored device performance. However, there are several disadvantages associated with plastic substrates, including a low processing temperature, a large coefficient of thermal expansion (CTE), and poor printability and recyclability. Processing on PET substrates is limited to 110 °C and that on PEN is limited to 160 °C. Polyimides can be processed up to 400 °C but the brown color makes them less attractive as a flexible and transparent substrate when a neutral color is required.

Recently, new biodegradable, flexible, and transparent substrates, including nanopaper and regenerated cellulose films (RCFs), have attracted much attention.[4,12–17] Plastic is made from the by-products of oil industries and is not renewable. Plastic cannot be decomposed through biodegradation in the same way as organic materials. It takes more than 30 years to decompose a plastic film container and 450 years for a plastic beverage bottle. Compared to plastic, it only takes 2–4 weeks to decompose a paper towel. Energy consumption is up to 1600 kW h per ton for nanocellulose fabrication.[39] Energy

[a]*Department of Materials Science and Engineering, University of Maryland, College Park, MD 20740, USA. E-mail: binghu@umd.edu*

[b]*Department of Mechanical and Materials Engineering, University of Nebraska-Lincoln, Lincoln, Nebraska 68588, USA*

[c]*State Key Laboratory of Pulp and Paper Engineering, South China University of Technology, Guangzhou 510640, China*

† Electronic supplementary information (ESI) available. See DOI: 10.1039/c3ee40492g

consumption for RCFs is much lower than that of nanocellulose. There is no need to go through homogenizer treatment for RCF fabrication, which is the main cause of energy consumption in nanocellulose preparation. Flexible substrates based on renewable materials could lead to truly green electronics. In addition, nanocellulose-based materials have been shown to be noncytotoxic. Regenerated cellulose is known to be compatible with human blood which opens up possibilities for exciting sustainable electronics applications in the biomedical field.[4,33] Transparent RCFs and transparent nanopaper made of biodegradable cellulose from nature were demonstrated.[9,14,18] The main difference between these two cellulose-based substrates is that nanopaper is comprised of one-dimensional nanofibers, whereas RCF is cast from fully dissolved cellulose. There has been little investigation, however, on these transparent substrates for device applications. A fundamental understanding and demonstration of device integration is needed for these biodegradable substrates to emerge as a viable replacement for the existing plastic substrates. This work focuses on the fundamental properties and comparison of the cellulose-based biodegradable transparent substrates as replacements for plastic substrates. Highly flexible OLED devices on the transparent nanopaper are also demonstrated.

Experimental

RCF preparation

0.7 g of cellulose fibers is dissolved completely in 24 g of 1-ethyl-3-methylimidazolium phosphorous methyl ester ionic liquid ($EMIMMeOPO_2H$) at 90 °C. The resulting liquid is poured into a glass-based cell to regenerate and subsequently washed with DI water. The RCF sample is then vacuum-dried at 20 °C for 10 h. The final RCF sample has dimensions of 80 mm length × 50 mm width × 1 mm thickness. Smaller RCF samples are also prepared with dimensions of 50 mm length × 30 mm width × 1 mm thickness.

$EMIMMeOPO_2H$ synthesis

The synthesis of $EMIMMeOPO_2H$ follows the methodology established previously.[19] Dimethyl phosphite is added dropwise to *N*-ethylimidazole–50 ml tetrahydrofuran (THF) solution in a glass-lined reactor under an argon gas atmosphere at room temperature. The molar ratio of dimethyl phosphite to *N*-ethylimidazole is 1 : 1.15. The mixture is stirred magnetically with reflux at 80 °C for about 48 h by SFT (Schlenk Flask Technology). After the chemical reaction is terminated, any residual THF is removed under reduced pressure. The resulting liquid is repeatedly washed with an excess amount of ether to eliminate the residual *N*-ethylimidazole, dimethyl phosphite, and any side reaction products. The remaining ionic liquid (IL) is dissolved completely in dichloromethane (CH_2Cl_2). The IL–CH_2Cl_2 solution is filtered through a glass filter filled with neutral activated alumina for purification. The resulting IL–CH_2Cl_2 solution is distilled under reduced pressure to remove the residual CH_2Cl_2. The pH value and zeta potential of the final IL are measured before drying under vacuum at 80 °C for 72 h with phosphorus pentoxide.

Nanopaper fabrication and characterization

2,2,6,6-Tetramethylpiperidine-1-oxyl (TEMPO, 78 mg) and sodium bromide (NaBr, 514 mg) are added to a pulp suspension (5 g of kraft bleached softwood pulp). TEMPO-mediated oxidation of the cellulose slurry is started by adding 12% NaClO at room temperature under gentle agitation. The pH is maintained at 10.5 by adding aqueous sodium hydroxide. After TEMPO treatment, the fibrous TEMPO-oxidized product is thoroughly washed with distilled water. A concentration of 1 wt% oxidized cellulose suspension is disintegrated by one pass through a Microfluidizer M-110EH (Microfluidics Ind., USA) to obtain an NFC suspension. The NFC suspension (0.2 wt%) is degassed with sonication and poured into a filter to obtain flexible and strong nanopaper. A multimode atomic force microscope (AFM) (Veeco Instruments) is used to characterize the surface of the nanopaper. The transmittance and haze of the nanopaper are obtained with a UV-vis spectrometer (Lambda 35, PerkinElmer, USA). The mechanical strength of the nanopaper is measured with a Tinius Olsen H25KT universal material strength testing machine. The machine is operated with headcross displacement control at a constant rate of 5 mm min^{-1} (with a strain rate of 20% per minute). The load cell has a maximum capacity of 25 kN and a minimum resolution of 0.83 N. The displacement measurement has a minimum resolution of 0.004 mm. Each specimen strip is cut to 5 mm × 50 mm. All specimens were conditioned for 24 h at 50% humidity and 23 ± 1 °C before testing.

OLED device fabrication

P3 SWNTs were purchased from Carbon Solutions (California, USA). 10 mg of CNTs is added to 10 ml of DI water with 1% SDBS (4-dodecylbenzenesulfonic acid), bath sonicated for 5 minutes, probe sonicated for 3 minutes, and finally purified using a centrifuge. In the end, 1 mg ml^{-1} SWNT ink is prepared. The CNT ink is coated on the nanopaper using a #18 Meyer rod (R. D. Specialties, Inc., USA). The hole transport layer is prepared by thermally evaporating 10 nm MoO_3 onto the nanopaper, and then spin coating 30 nm PEDOT:PSS at a speed of 2500 rpm. The substrate is then annealed at 135 °C for 30 min. Green polyfluorene solution with a concentration of 10 mg ml^{-1} is drop coated on top of the PEDOT:PSS layer and dried at 70 °C for 30 min in a N_2 filled glove box. The device is completed by thermally evaporating 20 nm Ca and 100 nm Al.

Results and discussion

Nanopaper and RCFs are new materials with high flexibility and optical transparency based on earth-abundant renewable materials. Both of them are made from cellulose, but their building blocks are different, as shown in Fig. 1. Nanopaper is made from nanofibrillated cellulose (NFC) fibers using a typical paper fabrication method. NFC is a natural nanomaterial that can be incorporated into a wide range of products to enhance their properties. There are several ways to prepare NFC, such as enzyme pretreatment, acid hydrolysis, ultrasonication, and homogenization.[20–23] In this work, the native wood fiber is pretreated with NaClO/NaBr/TEMPO, and

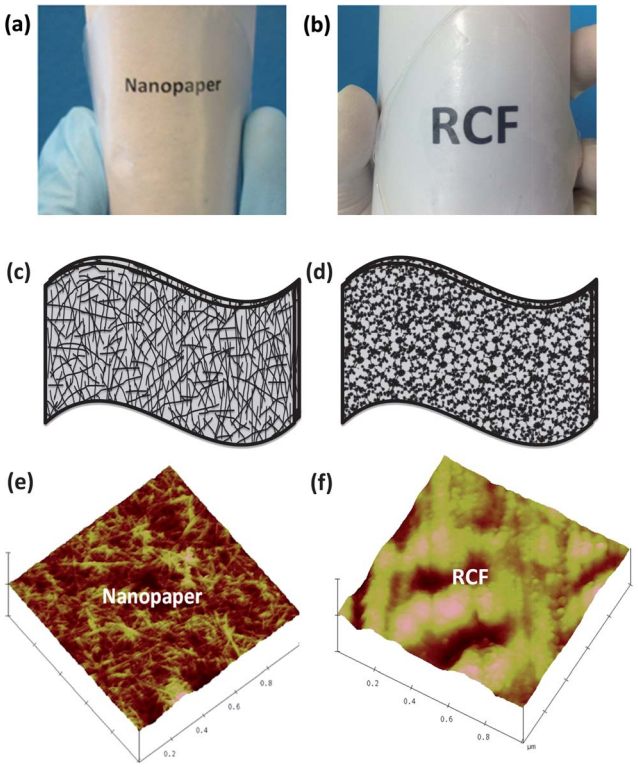

Fig. 1 Comparison of the nanopaper and regenerated cellulose film (RCF). Digital images showing the transparency and flexibility of the (a) nanopaper and (b) RCF. Schematics of (c) the nanopaper showing the nanofibrillated cellulose network and (d) the RCF cast from dissolved cellulose. Surface morphology studied by AFM for nanopaper (e) and RCF (f) at the scan size of 1 μm × 1 μm. The fibrous structure of the nanopaper is apparent.

then disintegrated with a microfluidizer. The obtained nanopaper possesses an NFC network as shown in Fig. 1(c). The high strength, high transparency, and high flexibility make it an excellent green substrate for electronics. Nanopaper can also be manufactured with higher haze, which is due to a large light scattering. The light scattering will lead to an anti-glare effect which is preferred in outdoor displays. RCF, shown in Fig. 1(b), (d) and (f), from sustainable wood materials was developed in the dissolving–regenerating process based on IL technology. The RCF is prepared by dispersing wood cellulose in a synthetic 1-ethyl-3-methylimidazolium phosphorous methyl ester ($EMIMMeOPO_2H$) IL to completely dissolve the cellulose, and subsequently regenerating and washing with DI water. Ionic liquids can be recycled 6–8 times.[38] In this process, the cellulose chains are reconstructed into a transparent film due to the establishment of new hydrogen bondings.[24]

Surface morphology affects many properties important for device applications. The surface roughness needs to be minimized to avoid shorting problems. The mechanical, optical, and electrochemical performances also closely depend on the structures of the substrates. We investigated the surface morphology of the two emerging transparent substrates, Fig. 1(e) and (f), with atomic force microscopy (AFM). Surface characterization of a PET substrate is provided in the ESI.† The diameter of NFC fibers used in nanopaper manufacturing can be tuned by preparation methods. In this study, the diameter of NFC fibers is 10 nm and the length is close to 500 nm. The mass density of nanopaper is found to be 1.2 g cm^{-3}, close to the reported value in the literature.[14,16,21,25–27] Fig. 1(f) shows the AFM image of RCF. The difference in surface structure between the RCF and nanopaper is drastic, although both are made of cellulose. The surface morphology of RCF more closely resembles that of a plastic substrate, without any of the fibrous structures observed in the nanopaper.

The surface RMS roughness was characterized by AFM with 5 μm × 5 μm areas of nanopaper, RCF, and PET is 7.7 nm, 6.8 nm, and 7.0 nm, respectively. For most flexible devices based on transparent substrates, the thickness of the active layer ranges from tens to hundreds of nanometers. The low surface roughness of these emerging substrates is comparable to that of widely used plastic substrates. Due to the fibrous structure, nanopaper contains nanoscale porosity which enhances liquid containment and transport and introduces new optical properties.

Organic optoelectronic devices require precise control of the optical properties of the substrate. Fundamentally different from plastic substrates, the optical properties of cellulose-based transparent substrates are tunable due to the availability of different building blocks derived from cellulose fibers with a hierarchical structure. The optical properties of the substrates were characterized with a UV-vis spectrometer. Specifically, we measured the diffusive and specular transmittance of the three different substrates. The diffusive transmittance incorporates all light transmitted in the forward direction, excluding any absorption or back scattering. The specular transmittance only includes light transmitted close to the direction perpendicular to a substrate. The difference between diffusive and specular transmittance is the amount of forward scattering off the normal direction. The results of UV-vis characterization of the three substrates with the same thickness (100 μm) are presented in Fig. 2. The transmittance results, Fig. 2(a) and (b), indicate that the nanopaper has the highest diffusive transmittance but the lowest specular transmittance. Transmittance for all the substrates is up to 90%, excellent for transparent substrate use. The sample thickness is much larger than the wavelength of light; the transmittance, therefore, is determined by the reflection index, the structure, and the surrounding materials. For plastic, there is little difference between the two types of transmittances indicating that plastic is superior for display applications. In applications where a high amount of scattering is desired, such as for solar cells and displays operating in a bright environment, plastic substrates are not ideal. RCF and nanopaper exhibit a much larger light scattering effect, indicated by the large difference between diffusive and specular transmittance. This is mainly due to the porous microstructures of the nanopaper and RCF. As the diameter for NFC in the nanopaper can range from 100 nm to 5 nm, the optical properties and surface roughness can be tailored further. This phenomenon will be described in future publications. When the diameter of NFC is in the range of a few nanometers, the

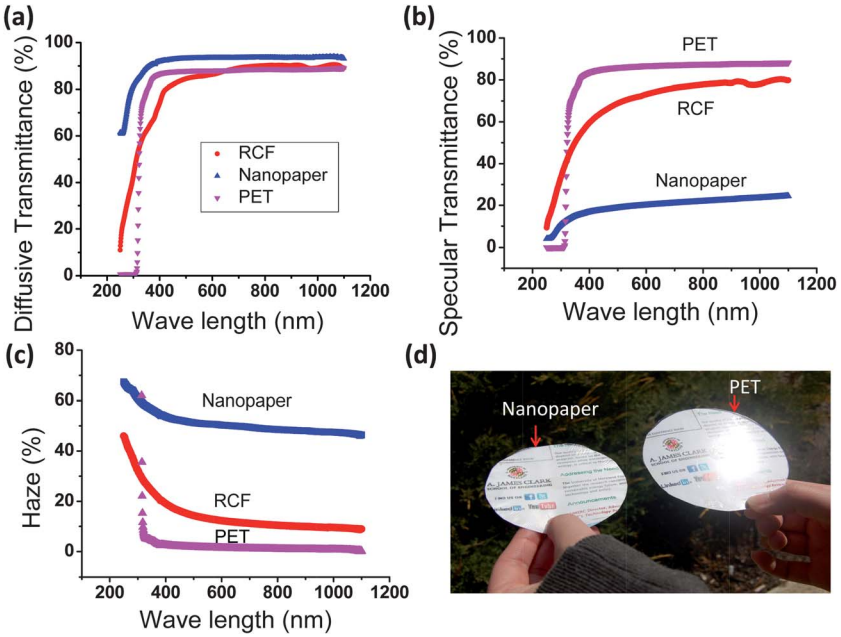

Fig. 2 Optical transmittance and haze comparison of nanopaper, RCF, and PET. (a) Diffusive optical transmittance (b) specular optical transmittance and (c) optical haze of the RCF, nanopaper, and PET substrates. (d) A digital image in the sunshine to illustrate the anti-glare effect of nanopaper substrates. The samples were held at the same angle to sunlight. Compared to PET, the nanopaper is more comfortable for people to read under sunshine.

difference between diffusive and specular transmittance is small and close to that of plastic.

A quantitative method to describe the light scattering of transparent substrates is the haze value. The haze value is defined as

$$\text{Haze} = \left[\left(\frac{T_4}{T_2}\right) - \left(\frac{T_3}{T_1}\right)\right] \times 100\%$$

where T_1 through T_4 are changing configurations of the sample placement on the UV-vis spectrum sphere. T_1 is the incident light, T_2 is the total transmitted illumination, T_3 is the light scattered by the instrument, and T_4 is the light scattered by the instrument and specimen. Fig. 2(c) shows the haze value in the visible and near infrared range. The PET substrate shows a much lower haze value than the nanopaper. For most of the wavelength range, the haze value is less than 5% for plastic. The value is up to 50% for nanopaper and for RCF it is much less in most of the wavelength range. The optical haze of the transparent nanopaper can be tuned by nanofiber diameters. RCF has an optical haze larger than 10% with worse clarity than plastic. The light scattering effect is shown clearly in Fig. 2(d). The plastic substrate has a large amount of glare, which is not observed for the nanopaper substrate. This is desirable for many display applications where operation in a bright environment is needed. Current technology utilizes anti-glare coatings, such as monolayer colloidal silicon nanoparticles.[28] The large light scattering and large haze values are important for light absorption in solar cells as the absorption path length is greatly increased.

For roll-to-roll processing of lightweight and flexible electronic devices, the mechanical properties of the substrates are important.[29] To study the effect of building block size on mechanical properties, we carried out stress–strain tests to evaluate the mechanical properties of nanopaper and RCF in detail. The tests were done with a tensile tester (Tinius Olsen H25KT). The samples were cut to dimensions of 5 mm × 50 mm. Fig. 3(a) shows the stress–strain curves for the three substrates. Transparent nanopaper has the highest tensile strength of 287 MPa, with a yield strength of 230 MPa and a Young's modulus of 9 GPa. RCF has a lower strength but larger strain than nanopaper. This is due to the differences in their microstructures. Nanopaper is made of NFC, in which interlocking fibers largely improve the mechanical properties. RCF, however, is based on the reestablishment of cellulose chains. The crystal structure of the cellulose in RCF is the cellulose II crystal structure, which is mechanically weaker than the cellulose I crystal structure of nanopaper.[17] The PET substrates exhibit an excellent strain performance up to 71%, but the tensile strength is less than that of the nanopaper.

The results of our characterization of the three substrates are carefully compared with other data reported in the literature.[17,27,30,31] Fig. 3(b) shows an Ashby plot of maximum stress *vs.* density. Nanopaper possesses a high strength but a low density, with a typical value of 0.64 g cm^{-3}. Its lightweight and high strength properties are extremely important for aerospace applications. Compared to cellulose substrates, PET has a higher density. The RCF has the lowest strength. Another important parameter for device stability and processing at elevated temperatures is the coefficient of thermal expansion (CTE). Fig. 3(c) shows an Ashby plot of CTE *vs.* Young's modulus for the three substrates. Nanopaper has the lowest CTE, followed by RCF and PET.[17] The difference between the RCF and nanopaper may be due to structural differences as their composition is the same. PET shows the worst

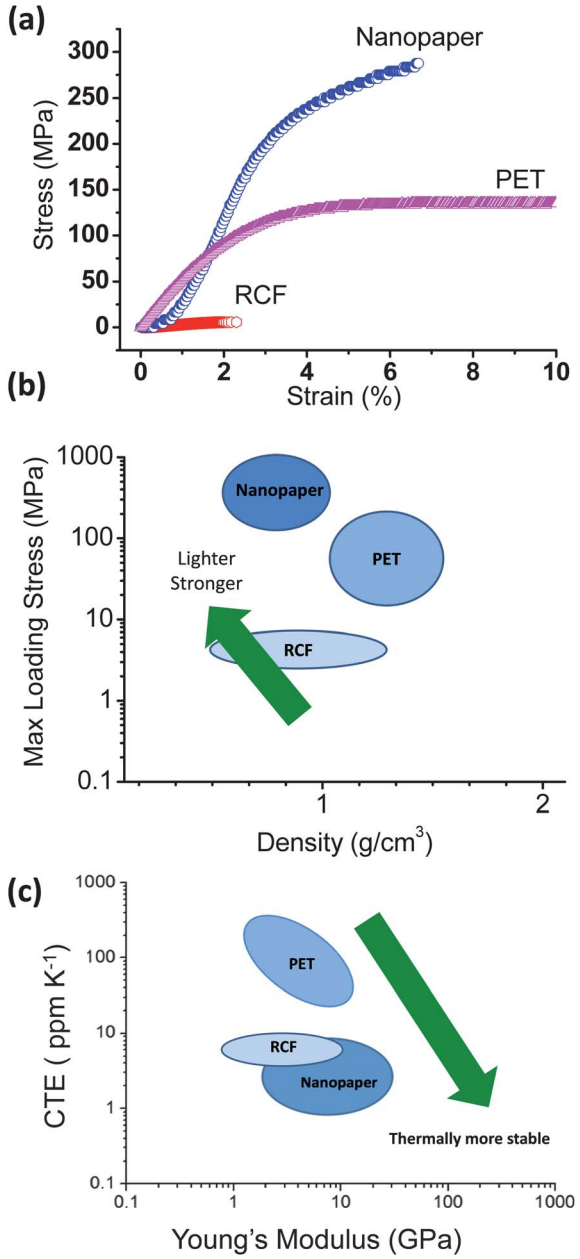

Fig. 3 Mechanical and thermal stability comparison of nanopaper, RCF, and PET. (a) Stress–strain curves of nanopaper, RCF, and PET. The nanopaper has the strongest tensile strength. Note that the maximum strain for PET is up to 81%. Ashby plots of (b) maximum loading stress *vs.* density, and (c) coefficient of thermal expansions *vs.* Young's modulus.

performance in terms of the combination of CTE and Young's modulus. This is one of the major motivations in the search for a replacement for device applications. This comparison of properties will be important as a reference for future device development on these substrates.

Table 1 shows the comparison of several important properties of nanopaper, RCFs and plastic. Compared to PET, the two cellulose substrates show excellent performance and are viable candidates for flexible electronic substrates. Nanopaper and RCF are based on renewable materials, which make them attractive for green electronics. The unique optical scattering

Table 1 Comparison of properties of nanopaper, RCF, and PET

Characteristics	Nanopaper	RCF	PET
Weight/density (g ml^{-1})	0.64	0.84	1.29–1.40
Elastic modulus (GPa)	7.4–14	7.3[32]	2–2.7
Coefficient of thermal expansion (ppm K^{-1})	2.7	10.3[32]	20–100
Maximum loading stress (MPa)	200–400	5.6	50–150
Strain at break	6–12	2.3	70
Maximum handling temperature (°C)	200	150	110
Optical transparency at 550 nm (%)	93	85	88
Bending radius (mm)	1	1	10
Cost	Potentially low	Moderate	Low
Renewable	High	High	Low

effect of nanopaper provides additional opportunities for use in low glare displays and printable solar cells. Due to the porous structure, nanopaper can also contain and transport liquids, a requirement for integration with batteries and microfluidic devices. The integration of electronic circuits and energy storage on a single sheet of nanopaper may be more feasible than using RCFs and plastic.

Based on biodegradable cellulose materials, both RCF and nanopaper are highly transparent, lightweight and highly flexible and are promising as substrates to replace plastic for electronic and optoelectronic device applications. Exploring the device applications of these biodegradable transparent substrates is in its infancy. Great challenges exist such as the morphology of materials after processing and substrate-active layer interfacial binding. One particular application is paper-OLEDs which are attractive for efficient lighting and displays. We will focus on the device study on nanopaper. Processes and fundamental knowledge can be extended to RCF substrates. As a demonstration, a highly flexible OLED device was fabricated on the nanopaper substrate. A schematic of the OLED device is provided in Fig. 4(a). Before fabrication of the device, the transparent nanopaper is made conductive by coating a carbon nanotube (CNT) film using the scalable Meyer rod coating method.[33–36] The sheet resistance of the CNT film is 200 Ohms per square. A scanning electron microscopy (SEM) image of the CNT-coated nanopaper is shown in Fig. 4(b). The transmittance of CNT-coated nanopaper is around 82% in the visible range as shown in Fig. 4(c), a transmittance comparable to commercial ITO substrates.

Fig. 4(d) shows the powered OLED on nanopaper. The device consists of a light emitting layer of green polyfluorene, a 10 nm molybdenum oxide (MoO_3) and 30 nm PEDOT:PSS (poly(3,4-ethylenedioxythiophene):poly(styrenesulfonate)) hole injection layer, and a 20 nm calcium (Ca) electron injection layer sandwiched between the anode (carbon nanotube) and cathode (aluminum). MoO_3 was deposited onto a CNT layer first as a wetting layer for PEDOT:PSS and the light emitting layer. A thick light emitting layer of around 300 nm, prepared by drop coating, was used to eliminate any shorting of the device. Detailed OLED fabrication procedures are provided in the

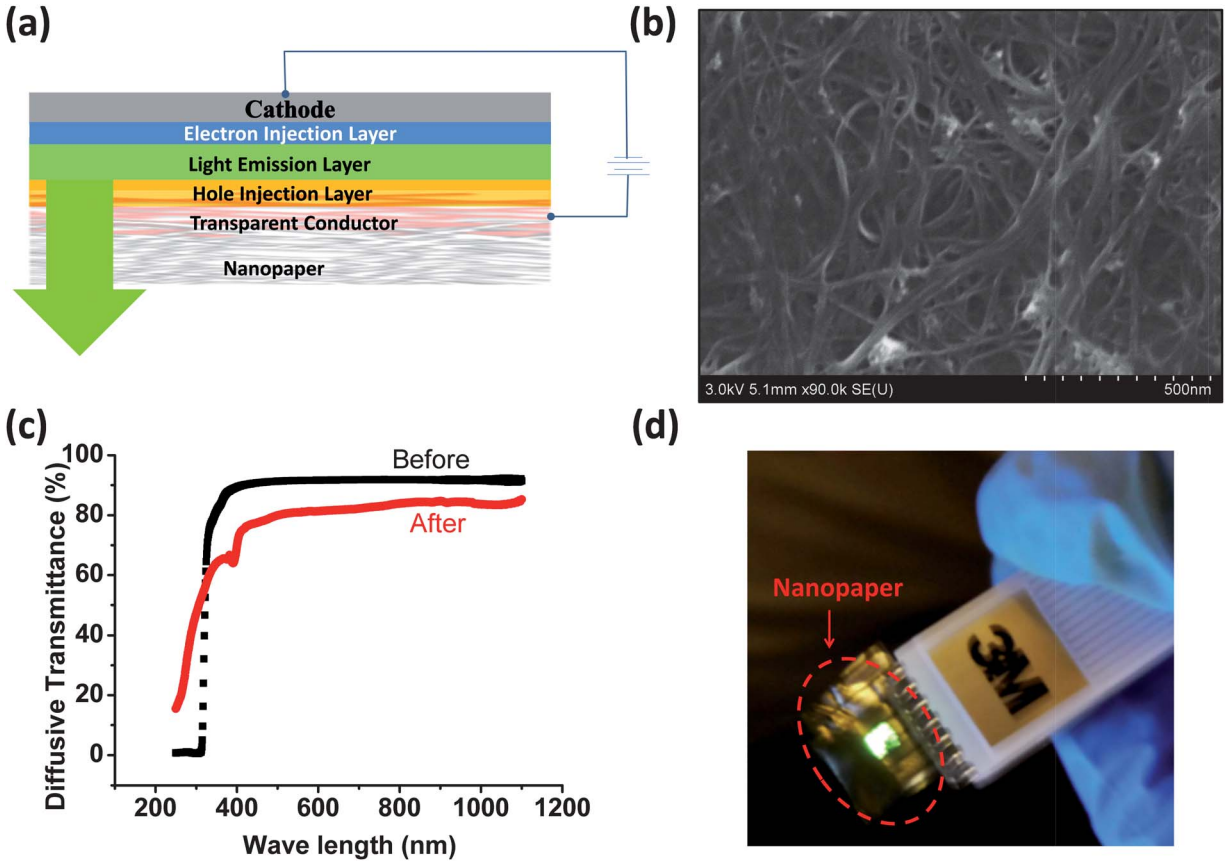

Fig. 4 A transparent and flexible OLED device on a nanopaper substrate. (a) Schematic drawing of a nanopaper OLED device. (b) SEM image of CNTs on transparent nanopaper. (c) Total transmittance before and after CNT coating. (d) Picture of the OLED in operation.

Experimental section. Under forward bias, photons are generated *via* radiative recombination of the injected electrons and holes in the light emitting layer, causing the device to light up as shown in Fig. 4(d).

To demonstrate the excellent flexibility of the fabricated OLEDs on the nanopaper, the current density *versus* voltage (*J*–*V*) curve of an OLED device was characterized by bending the device with a radius of 1.5 mm. The device pictures in the flat and bent states are shown in Fig. 5(a) and (b), and the corresponding *J*–*V* curves are shown in Fig. 5(c). There is little difference between the *J*–*V* curves before and after bending the device. It should be noted that the relatively large bias of the device is caused by the relatively thick emission layer and the low conductance of the CNT layer. This experiment demonstrates that nanopaper is an extremely promising substrate for flexible electronics. Compared with plastic substrates, fibrous nanopaper substrates could potentially release the stress during bending more effectively, which may enable more flexible, even bendable devices. Further study will focus on reducing the thickness of the organic light emitting layer without shorting the device, and improving the conductivity of the CNT layer without sacrificing its transmittance. The fibrous structure of nanopaper is fundamentally different from that of plastic, and could release the stress and avoid cracking typically observed in plastic based flexible electronics.[37]

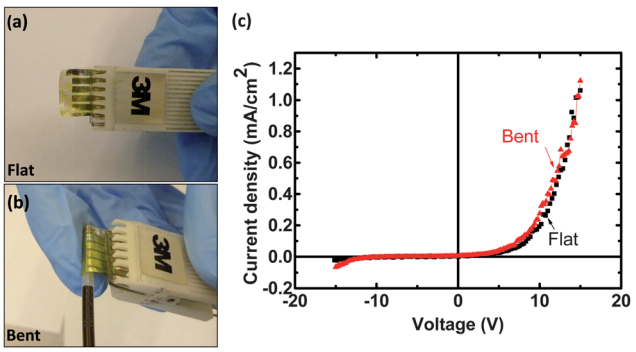

Fig. 5 Nanopaper OLED flexibility test: pictures of the (a) flat and (b) bent nanopaper OLED device. (c) *J*–*V* curve of the flexible OLED in the flat and bent states, respectively. The bending radius is 1.5 mm.

Conclusions

We have evaluated and compared several properties of nanopaper and RCFs, along with traditionally used flexible plastic, for use as flexible electronic substrates. We found that both RCFs and nanopaper are highly transparent in the visible and near infrared wavelength regions. All three substrates possess a surface roughness less than 20 nm, making them suitable for printed electronic devices. Additionally, these substrates are all flexible enough to be compatible with roll-to-roll processing.

Although both nanopaper and RCF are made from cellulose, the difference in their microstructures leads to a large difference in their optical and mechanical properties. In particular, the nanopaper possesses a much higher haze value, ideal for low glare displays and solar cells. An OLED device fabricated on nanopaper was demonstrated and the performance was found to be stable in both the flat and bent state. This study is important for the future development of flexible electronics based on new transparent substrates.

Acknowledgements

We acknowledge the use of the Modern Engineering Materials Instructional Laboratory (MEMIL) at the University of Maryland for mechanical testing and the sharing of the Microfluidizer at the Biotechnology Research and Education Center. L. Hu acknowledges the startup support from the University of Maryland, College Park. We acknowledge the support of the Maryland NanoCenter and its NispLab. The NispLab is supported in part by the NSF as a MRSEC Shared Experimental Facility. J. Huang acknowledges the financial support from the National Science Foundation under Award ECCS-1201384 and ECCS-1252623, and the Nebraska Public Power District through the Nebraska Center for Energy Sciences Research.

Notes and references

1 P. C. Chen, Y. Fu, R. Aminirad, C. Wang, J. L. Zhang, K. Wang, K. Galatsis and C. W. Zhou, *Nano Lett.*, 2011, **11**, 5301–5308.
2 B. Liu, J. Zhang, X. F. Wang, G. Chen, D. Chen, C. W. Zhou and G. Z. Shen, *Nano Lett.*, 2012, **12**, 3005–3011.
3 L. Hu, H. S. Kim, J.-Y. Lee, P. Peumans and Y. Cui, *ACS Nano*, 2010, **4**, 2955–2963.
4 D. O. Carlsson, G. Nystrom, Q. Zhou, L. A. Berglund, L. Nyholm and M. Stromme, *J. Mater. Chem.*, 2012, **22**, 19014–19024.
5 V. Zardetto, T. M. Brown, A. Reale and A. Di Carlo, *J. Polym. Sci., Part B: Polym. Phys.*, 2011, **49**, 638–648.
6 W. J. Yu, S. Y. Lee, S. H. Chae, D. Perello, G. H. Han, M. Yun and Y. H. Lee, *Nano Lett.*, 2011, **11**, 1344–1350.
7 V. Scardaci, R. Coull and J. N. Coleman, *Appl. Phys. Lett.*, 2010, **97**, 023114–023116.
8 A. R. Rathmell and B. J. Wiley, *Adv. Mater.*, 2011, **23**, 4798–4803.
9 M. Nogi, S. Iwamoto, A. N. Nakagaito and H. Yano, *Adv. Mater.*, 2009, **21**, 1595–1598.
10 L. Hu, H. Wu and Y. Cui, *MRS Bull.*, 2011, **36**, 760–765.
11 A. Anctil, C. W. Babbitt, R. P. Raffaelle and B. J. Landi, *Prog. Photovoltaics*, 2012, DOI: 10.1002/pip.2226.
12 E. Fortunato, N. Correia, P. Barquinha, L. Pereira, G. Goncalves and R. Martins, *IEEE Electron Device Lett.*, 2008, **29**, 988–990.
13 A. N. Nakagaito, M. Nogi and H. Yano, *MRS Bull.*, 2010, **35**, 214–218.
14 M. Nogi and H. Yano, *Appl. Phys. Lett.*, 2009, **94**, 23117–23119.
15 H. Yano, J. Sugiyama, A. N. Nakagaito, M. Nogi, T. Matsuura, M. Hikita and K. Handa, *Adv. Mater.*, 2005, **17**, 153–155.
16 S. J. Eichhorn, A. Dufresne, M. Aranguren, N. E. Marcovich, J. R. Capadona, S. J. Rowan, C. Weder, W. Thielemans, M. Roman, S. Renneckar, W. Gindl, S. Veigel, J. Keckes, H. Yano, K. Abe, M. Nogi, A. N. Nakagaito, A. Mangalam, J. Simonsen, A. S. Benight, A. Bismarck, L. A. Berglund and T. Peijs, *J. Mater. Sci.*, 2010, **45**, 1–33.
17 R. J. Moon, A. Martini, J. Nairn, J. Simonsen and J. Youngblood, *Chem. Soc. Rev.*, 2011, **40**, 3941–3994.
18 Q. L. Yang, X. Z. Qin and L. N. Zhang, *Cellulose*, 2011, **18**, 681–688.
19 Y. Fukaya, K. Hayashi, M. Wada and H. Ohno, *Green Chem.*, 2008, **10**, 44–46.
20 P. B. Filson, B. E. Dawson-Andoh and D. Schwegler-Berry, *Green Chem.*, 2009, **11**, 1808–1814.
21 T. Saito, S. Kimura, Y. Nishiyama and A. Isogai, *Biomacromolecules*, 2007, **8**, 2485–2491.
22 L. Wagberg, G. Decher, M. Norgren, T. Lindstroem, M. Ankerfors and K. Axnaes, *Langmuir*, 2008, **24**, 784–795.
23 A. D. Liu, A. Walther, O. Ikkala, L. Belova and L. A. Berglund, *Biomacromolecules*, 2011, **12**, 633–641.
24 D. T. Liu, K. F. Xia, W. H. Cai, R. D. Yang, L. Q. Wang and B. Wang, *Carbohydr. Polym.*, 2012, **87**, 1058–1064.
25 S. J. Chun, S. Y. Lee, G. H. Doh, S. Lee and J. H. Kim, *J. Ind. Eng. Chem.*, 2011, **17**, 521–526.
26 H. Fukuzumi, T. Saito, T. Wata, Y. Kumamoto and A. Isogai, *Biomacromolecules*, 2009, **10**, 162–165.
27 H. Sehaqui, Q. Zhou, O. Ikkala and L. A. Berglund, *Biomacromolecules*, 2011, **12**, 3638–3644.
28 K. Askar, B. M. Phillips, X. Dou, J. Lopez, C. Smith, B. Jiang and P. Jiang, *Opt. Lett.*, 2012, **37**, 4380–4382.
29 N. Cordero, J. Yoon and Z. Suo, *Appl. Phys. Lett.*, 2007, **90**, 111910–111913.
30 H. Sehaqui, N. E. Mushi, S. Morimune, M. Salajkova, T. Nishino and L. A. Berglund, *ACS Appl. Mater. Interfaces*, 2012, **4**, 1043–1049.
31 Q. Zhang, G. H. Wu, G. Q. Chen, L. T. Jiang and B. F. Luan, *Composites, Part A*, 2003, **34**, 1023–1027.
32 Q. L. Yang, S. Fujisawa, T. Saito and A. Isogai, *Cellulose*, 2012, **19**, 695–703.
33 N. Ferraz, D. O. Carlsson, J. Hong, R. Larsson, B. Fellström, L. Nyholm, M. Strømme and A. Mihranyan, *J. R. Soc., Interface*, 2012, **9**, 1943–1955.
34 J. Krantz, M. Richter, S. Spallek, E. Spiecker and C. J. Brabec, *Adv. Funct. Mater.*, 2011, **21**, 4784–4787.
35 B. Dan, G. C. Irvin and M. Pasquali, *ACS Nano*, 2009, **3**, 835–843.
36 X. Li, F. Gittleson, M. Carmo, R. C. Sekol and A. D. Taylor, *ACS Nano*, 2012, **6**, 1347–1356.
37 J. Huang, H. Zhu, Y. Chen, K. Rohrbach and L. Hu, *ACS Nano*, 2013, **7**(3), 2106–2113.
38 B. Li, J. Asikkala, I. Filpponen and D. S. Argyropoulos, *Ind. Eng. Chem. Res.*, 2010, **49**, 2477–2484.
39 H. L. Zhu, M. Helander, C. Moser, A. Stahlkranz, D. Soderberg, G. Henriksson and M. Lindstrom, *Curr. Org. Chem.*, 2012, **16**, 1871–1875.